

Incoherent phonon population and exciton-exciton annihilation in monolayer WS₂ revealed by time-resolved spontaneous Raman scattering

Shuangping Han,^{1, 3} Christoph Boguschewski,² Yan Gao,*^{1, 3} Liantuan Xiao,^{1, 3} Jingyi Zhu² and Paul H. M. van Loosdrecht*²

¹ State Key Laboratory of Quantum Optics and Quantum Optics Devices, Institute of Laser Spectroscopy, Shanxi University, Taiyuan, Shanxi 030006, China.

² Physics institute 2, University of Cologne, 50937, Germany.

³ Collaborative Innovation Center of Extreme Optics, Shanxi University, Taiyuan, Shanxi 030006, China.

E-mail: ago@sxu.edu.cn

pvl@ph2.uni-koeln.de

Abstract

Atomically thin layer transition metal dichalcogenides have been intensively investigated for their rich optical properties and potential applications in nano-electronics. In this work, we study the incoherent optical phonon and exciton population dynamics in monolayer WS₂ by time-resolved spontaneous Raman scattering spectroscopy. Upon excitation of the exciton transition, both the Stokes and anti-Stokes optical phonon scattering strength exhibit a large reduction. Based on the detailed balance, the optical phonon population is retrieved, which shows an instant build-up and a relaxation lifetime of ~ 4 ps at an exciton density $\sim 10^{12}$ cm⁻². The corresponding optical phonon temperature rises by 25 K, eventually, after some 10's of picoseconds, leading to a lattice heating by only ~ 3 K. The exciton relaxation dynamics extracted from the transient vibrational Raman response shows a strong excitation density dependence, signaling an important bi-molecular contribution to the decay. The exciton relaxation rate is found to be $\sim (70 \text{ ps})^{-1}$ and exciton-exciton annihilation rate $\sim 0.1 \text{ cm}^2\text{s}^{-1}$. These results provide valuable insight into the thermal dynamics after optical excitation and enhance the understanding of the fundamental exciton dynamics in two-dimensional transition metal materials.

Keywords: Monolayer WS₂, Transient Raman spectroscopy, phonon population, exciton-exciton annihilation

1. Introduction

While the rise of graphene materials [1] and its research are still booming, various other atomically thin materials have emerged, sparking a novel and fascinating field of research [2, 3]. Among them, monolayer transition metal dichalcogenides (TMDCs) play an important role, arising from the intriguing physical properties rooted in their electronically gapped nature, reduced dimensionality, and lack of inversion and time reversal symmetry. TMDCs are regarded by many as a new generation of functional materials with a strong potential for applications in optoelectronic devices [4-9].

One of the significant differences between monolayer TMDCs and graphene is that the former shows an intrinsic band gap, with transition energies ranging from the visible into the near infrared. Rather than free carrier excitations, the lowest energy electronic excitations are strongly bound electron-hole pairs, i.e. excitons with large binding energies up to a few hundred meV [10-13]. These excitonic transitions provide an ideal platform for the study of exciton properties and the related optically induced dynamics in two dimensional semiconductors. This is not only of strong interest from a fundamental materials science point of view, but is also pivotal in eventually realizing the application potential of TMDCs. Not surprisingly, the properties induced by optical excitation and the associated relaxation dynamics in TMDCs have been extensively studied in the recent past using a variety of ultrafast spectroscopic techniques [14-25]. These studies revealed a number of interesting properties, including a giant optically induced band gap renormalization [19, 20, 25] leading to a pronounced spectral dynamics, a strong valley-selective optical Stark effect [26-28], which is of interest in view of optical control in possible valleytronics applications, and a strong material and excitation dependence of the exciton relaxation dynamics showing timescales ranging from tens to hundreds of picoseconds originating from both first and second order relaxation processes [16, 18, 21, 22, 24].

Whereas previous ultrafast spectroscopic studies on monolayer TMDCs mainly focused on the electronic excitation aspects, the lattice and thus the phonon population dynamics, which play a crucial role in the energy dissipation after optical excitation, have not yet been investigated in a direct manner [29]. Time-resolved spontaneous Raman spectroscopy (TRSRS) can provide a direct

access to study both the incoherent phonon relaxation as well as the electron-phonon coupling dynamics [30-34]. Recently we have demonstrated that not only the optical phonons but also the exciton population dynamics can be detected by monitoring the optical induced differential Stokes and anti-Stokes Raman signals in one-dimensional graphene nanoribbons [35]. Especially, under a strongly resonant Raman probing condition, the exciton dynamics can be directly obtained from the differential Stokes signal due to its relatively weak dependence on the induced changes in the phonon population. Here we report on an investigation of the phonon creation and relaxation dynamics as well as the exciton relaxation and annihilation mechanisms in monolayer WS₂ using TRSRS. The observed fast optical phonon population and depopulation dynamics show an efficient electron-lattice and optical-acoustical phonon coupling leading to fast initial energy dissipation after optical excitation. The observed exciton relaxation time depends strongly on density of optically excited excitons, demonstrating that exciton-exciton annihilation contributes strongly to the exciton relaxation dynamics in monolayer WS₂.

2. Experimental methods

Monolayer WS₂ samples were produced through chemical vapor deposition (CVD) [36, 37] on an oxide coated (280 nm) silicon substrate. The sample was characterized using atomic force microscopy (AFM), steady state photoluminescence and standard Raman spectroscopy, demonstrating the high quality of our sample. The standard Raman and photoluminescence spectra were recorded using a micro-Raman setup equipped with a triple stage spectrometer (Spectroscopy & Imaging GmbH) and LN₂ cooled CCD detector (PyLoN 100; Princeton Instruments). A picosecond laser (515 nm, ~ 2 ps) was used for the standard Raman and luminescence measurements. The 515 nm laser pulse was spectrally cleaned and narrowed (full width a half maximum (FWHM) ~10 cm⁻¹) using a home build pulse shaper. The laser pulses were focused on the sample using microscope objective (20×, NA=0.4). The Raman or photoluminescence signals of WS₂ were collected in a backscattering geometry.

Details of the TRSRS technique used here and related data analysis methods have been described elsewhere [38]. Briefly, an integrated ultrafast laser system (Light Conversion PHAROS) with two outputs of the fundamental pulses (300 fs and 150 ps, @1030 nm) pump two optical parametric amplifiers (Light Conversion), one to generate laser pulses for selective excitation (~300 fs), and one to generate a narrow-bandwidth laser pulse for Raman probing (~2 ps). For excitation of the WS₂ sample, the pump pulse wavelength was centered at ~ 620 nm (2.0 eV),

corresponding to the direct A exciton resonance. The Raman probe pulse was set at 515 nm (2.4 eV), in resonance with the B excitonic transition [12]. This configuration of pump and probe yields a strong resonant Raman probing signal and a direct excitation of excitons with only a small amount of excess energy. In order to minimize the background scattering induced by the relatively strong pump pulse, a crossed linear polarization of pump and probe was used, while detecting the Raman signal polarized parallel to the probe pulse.

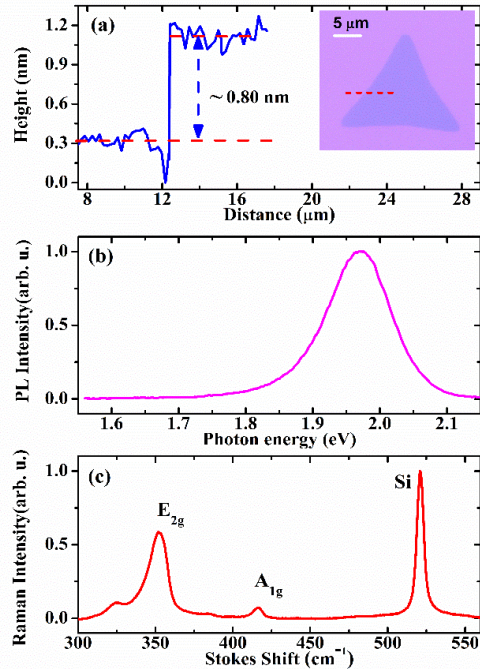


Fig. 1 Steady state spectra characterization of the CVD grown monolayer WS₂ sample on silica/silicon substrate. (a) Atomic force microscope (AFM) measurement the thickness of monolayer WS₂, inset show the optical image and AFM scanning range (dashed red line). (b) Photoluminescence. (c) Steady Raman scattering.

3. Results and discussion

The inset of Fig. 1(a) shows an optical image of the triangularly shaped crystalline monolayer WS₂ sample. The main panel 1(a) presents an AFM line scan along the dashed line in the inset image, showing the for a monolayer expected thickness of roughly 0.8 nm [39]. The monolayer quality of the sample was further confirmed by the steady state photoluminescence (PL) and Raman spectra presented in Fig. 1 (b) and (c), respectively. The PL spectrum has a peak located around 1.97 eV, corresponding to the excitonic A transition of crystalline single layer WS₂ [39, 40]. The slight broadening of the PL spectrum and the asymmetric peak shape with weaker tails extending towards the lower energy side is due to structural defects inducing different charged exciton

contributions [41-43]. The Raman spectrum shows a strong response at 350 cm^{-1} , corresponding to an E_{2g} in-plane optical phonon mode and a weaker mode at 415 cm^{-1} originating from either the out-plane vibration or from defect modes [44-46]. The peak located at 520 cm^{-1} is due to the underlying silica/silicon substrate. The peak positions and the relative ratio of peak intensities are in good agreement with previously reported Raman spectra of monolayer WS_2 on silica/silicon substrate [47, 48]. In the time-resolved measurements, we focus on the dynamic changes induced on the strongest in-plane mode (E_{2g}) at around 350 cm^{-1} .

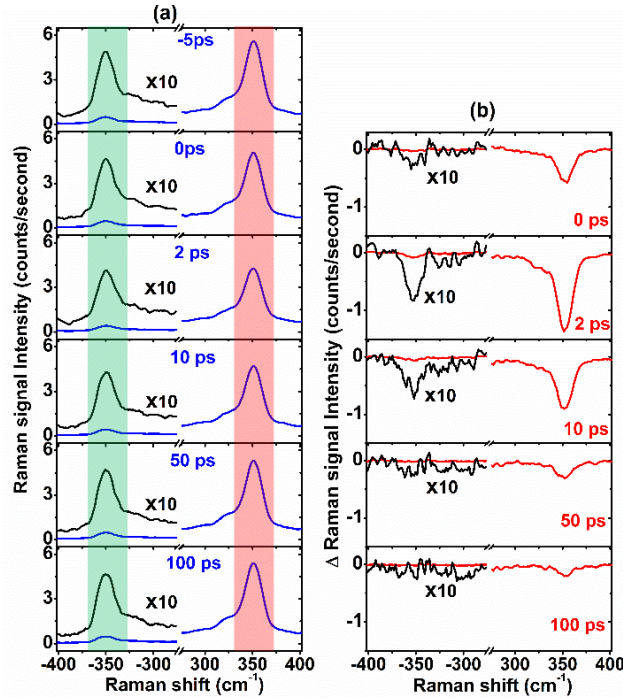


Fig. 2 Time-resolved spontaneous Raman scattering spectra of the monolayer WS_2 on silica/silicon recorded on both Stokes and anti-Stokes sides simultaneously. (a) Raman scattering intensity spectra at different delay times after optical pump at 2.0 eV . (b) Pump induced difference spectra obtained by subtraction the spectrum at -5 ps from each spectrum in (a) at different corresponding delay times.

Time-resolved spontaneous Raman scattering spectra of monolayer WS_2 around the 350 cm^{-1} E_{2g} phonon response are presented in Fig. 2. Fig. 2(a) shows the transient Stokes and anti-Stokes spectra for various pump-probe delay times using an initial photo-excited exciton density of $\sim 2.26 \times 10^{12}\text{ cm}^{-2}$, whereas Fig.2(b) shows the derived difference spectra obtained by subtracting the response at -5 ps (top panel Fig. 2(a)). From these spectra it is clear that the optical pump induces a significant reduction of the scattering efficiency, without any spectral dynamics of broadening or shifting, which recovers on a time scale of tens of ps. As we have discussed previously for the resonant Raman scattering case [35] the induced transient changes may originate both from

changes in the resonant enhancement due to electronic population effects (typically leading to a reduction of the response) as well as from changes in the vibrational population (typically leading to an increase of the response). Normally semiconductors show an induced increase of the anti-Stokes Raman signals [30, 31, 33-35, 38, 49, 50] assigned to a dominated contribution of optical phonon populations, and an increase or decrease of the Stokes scattering depending on resonance conditions. For monolayer WS₂, however, this is not the case. Here both Stokes and anti-Stokes scattering show a transient decrease, suggesting a dominating contribution from transient changes in the electronic resonance enhancement overshadowing the phonon population contribution on both sides.

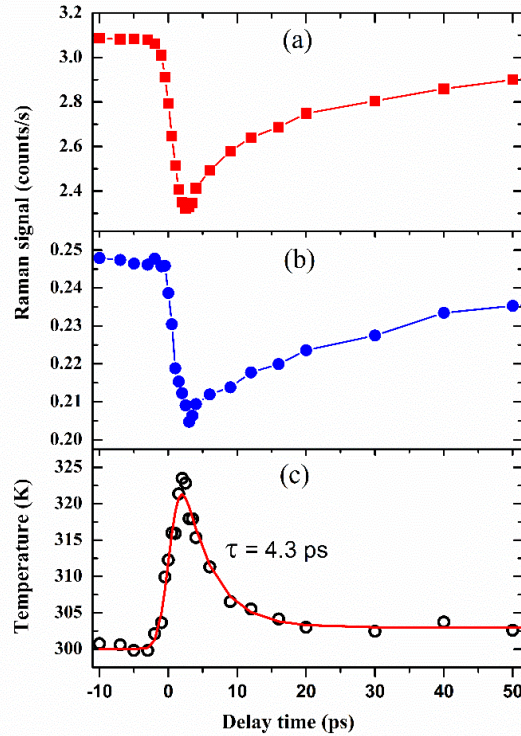


Fig. 3 Decay dynamics of the optical phonon peak at around 350 cm^{-1} at the exciton density around $2.26 \times 10^{12} \text{ cm}^{-2}$. (a) Stokes side dynamics integrated in the spectral region from 338 to 362 cm^{-1} . (b) Anti-Stokes side dynamics integrated in the spectral region from -362 to -338 cm^{-1} . (c) Calculated temperature of the optical phonon according to Bose-Einstein statistics.

To obtain a better view on the detailed relaxation dynamics of the optical phonon scattering, the E_{2g} phonon peak at $\sim 350 \text{ cm}^{-1}$ was spectrally integrated (green and red bar indicated in Fig. 2(a)) for different delay times. The obtained decay dynamics are presented in Fig. 3 for the Stokes (a) and anti-Stokes (b) responses. Though both anti-Stokes and Stokes sides show a transient

reduction with a recovery time of some 10s of ps, the detailed transient response is substantially different, in particular at early times. The origin of this difference is the (positive) contribution of the phonon population to the response, in particular for the anti-Stokes signal. In order to retrieve the optical phonon population dynamics, we assume that shortly ($<1\text{ps}$) after optical excitation the fluctuation-dissipation theorem holds and the ratio between Stokes and anti-Stokes scattering is given by

$$I_S / I_{AS} = \eta \cdot \exp(h\Omega/k_B T), \quad (1)$$

in which h is the plank constant, Ω is the optical phonon frequency, k_B is the Boltzmann constant and T is the phonon temperature. The prefactor η summarizes differences in for instance resonance enhancement [51, 52] and optical material properties [53, 54], and can be determined from an experiment at a known temperature. To determine η , we further make the assumption that before time zero, the phonon temperature is close to the environment ($\sim 300\text{ K}$). This assumption is reasonable in view of the low Raman probe laser pulse fluence, and the observation that there are no significant differences between pre-zero delay time intensities measured with and without the presence of the pump laser beam.

The transient phonon temperature determined using Eq. (1) presented in Fig. 3(c) shows an instantaneous (within our time resolution) increase by about 25 K, corresponding to a transient increase of the optical phonon population. The increased phonon population relaxes with a decay time of 4.3 ps to a long lived quasi equilibrium state with a temperature of about 3 K above base temperature, which further relaxes to the base temperature outside our detection time window but within the time between two pump pulses (10 μs).

The observation of the fast ($<2\text{ps}$) rise in phonon temperature after excitation suggests that optical phonon populations are created through a fast exciton-phonon scattering process, This can be either thorough release of the excess energy of the optically excited exciton states, or through transitions from the optically excited bright exciton states into optically inactive dark exciton states. In monolayer WS_2 the dark exciton state is formed by the electrons in the conduction band and holes in the valence band with opposite spins, and the energy of this dark exciton state is slightly lower (30-50 meV) than the bright exciton state [55-59]. Since relaxation from the bright to the dark exciton state requires a spin flip of the electrons, this process is expected to be substantially slower than the exciton cooling process but cannot be excluded on the basis of the current

experiments. The relaxation of the optical phonon population (~ 4.3 ps) can be ascribed to optical-acoustic phonon scattering usually occurring on a timescale of a few ps in semiconductors [30, 31, 33-35, 38, 49].

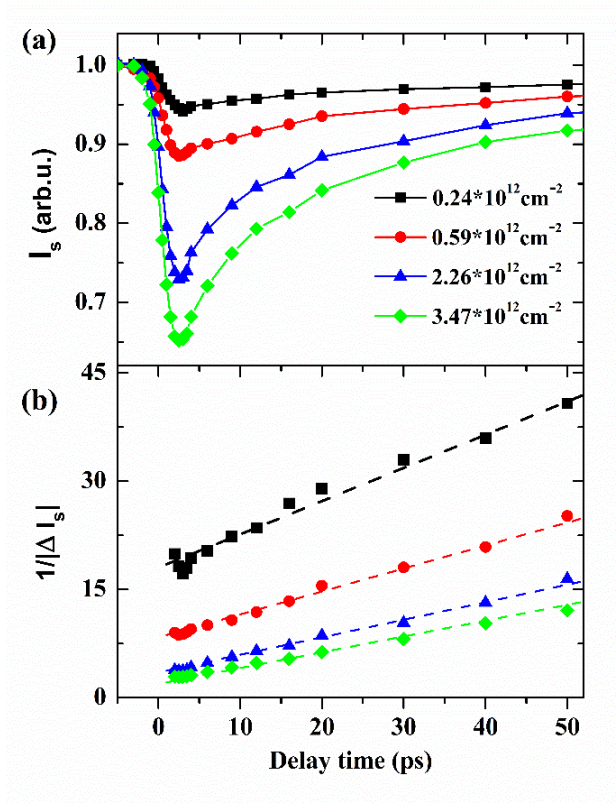


Fig. 4 Intensity dependence of the dynamics observed on Stokes side. (a) Decay dynamics of the optical phonon peak at around 350 cm^{-1} at different exciton density. (b) Inversion of the decay dynamics (dots) from (a) and the global fitted ones (dashed lines) with rate equation including both the first and second order exciton annihilation reaction (details see text in the paper). The global fitting extracted rate constants of $k_1 \sim (67 \text{ ps})^{-1}$ and $k_2 \sim 0.104 \text{ cm}^2\text{s}^{-1}$.

Apart from information on the phonon population dynamics and lattice temperature, one can straight forwardly derive the exciton population dynamics from the resonant TRSRS experiment. This is done by analyzing the time resolved optical phonon Stokes scattering signal, which is hardly influenced by the minor changes in total phonon population induced by the pump pulse.[35,38] The observed transient changes in the Stokes response can be ascribed to changes in the resonance enhancement due to ground state bleaching/excited state filling by the pump pulse, i.e. due to a transient reduction of the optical transition probability. The 10s of ps recovery time of the phonon signals is therefore assigned to relaxation of the excited excitonic states. In order to get a better insight into the exciton relaxation dynamics we performed a set of experiments for varying initial

exciton densities. Fig. 4a shows the integrated E_{2g} mode Stokes side signal for different excitation densities. The data show a clear speed up of the recovery dynamics upon increasing excitation density, indicating that many body annihilation processes play a role in the decay dynamics.

To analyse the observed phenomena, we model the dynamics by including both a first order free exciton decay process and a second order relaxation process, i.e., exciton-exciton annihilation. The population decay can then be expressed as:

$$dN(t)/dt = -k_1N(t) - k_2N^2(t), \quad (2)$$

where $N(t)$ is the time dependent exciton population density, and k_1 (k_2) is the first (second) order rate constant. Analytically solving (2) gives

$$1/N(t) = [1/N(0) + k_2/k_1] \exp(k_1 t) - k_2/k_1, \quad (3)$$

in which $N(0)$ is the initially excited exciton density. Since the effective lifetime from the first order reaction is usually much longer than that from the second order one, to simplify the description, in short time range, we expand $\exp(k_1 t)$ to $1 + k_1 t$ and (3) becomes:

$$1/N(t) = 1/N(0) + [k_1/N(0) + k_2]t \quad (4)$$

Expression (4) gives a very compact and intuitive description for the observed signals: it indicates that the inverse of the differential Raman signals should be simply linearly proportional to the delay time t , while the slope is excitation density dependent. Indeed, as shown in Figure 4(b), this is exactly the case here. Global fitting (dashed lines) of the data (symbols) using Expression (4) yields satisfactory agreement and a first order rate constant $k_1 = (67 \text{ ps})^{-1}$ and second order $k_2 = 0.104 \text{ cm}^2\text{s}^{-1}$. These values are comparable to those reported for other measurements on CVD grown monolayer WS₂ samples [21, 22], confirming the importance of an efficient exciton-exciton annihilation process in monolayer WS₂. The slight difference of the rate constants observed here and those in previous experiments on CVD grown samples are most likely due to variations in defect densities. We note that the values reported for CVD grown samples differ substantially from those measured on exfoliated samples. In exfoliated monolayer WS₂, the first order exciton decay rate constant was measured to be around $(806 \text{ ps})^{-1}$, one order slower, while the exciton-exciton annihilation rate k_2 was around $0.41 \text{ cm}^2\text{s}^{-1}$, 4 times larger [18]. The typical defect density ($\sim 3 \times 10^{13} \text{ cm}^{-2}$) [60] in a CVD grown sample is usually much higher than that in exfoliated samples ($\sim 2 \times 10^9 \text{ cm}^{-2}$) [61], This difference strongly influences the diffusion of excitons [62] and thus affects both

the first and second order decay processes, leading to a larger k_1 due to defect assisted recombination [63, 64] and a smaller k_2 due to slower diffusion in CVD grown WS_2 . These results suggest that the quantum efficiency of light emission and thermal effects caused by strong excitation conditions may be optimized for optical device applications by manipulating the defects density in the fabrication process of TMDCs.

4. Conclusion

In conclusion we have investigated the relaxation dynamics of both the phonons and excitons after optical excitation in a CVD grown monolayer WS_2 using TRSRS spectroscopy. The population the E_{2g} optical phonon shows a very fast (<2 ps) increase due to efficient exciton-phonon coupling and decays with time constant of around 4 ps through optical-acoustic phonon scattering. The exciton relaxation and annihilation dynamics, as observed through the time dependent Stokes optical phonon signals show the presence of both first and second order decay processes. The first order and the second order exciton decay rates obtained from the experiments are consistent with those obtained by other methods for CVD grown samples, but differ substantially from those for exfoliated samples due to the higher defect density. The present results provide a direct insight into both the excitonic and vibrational energy dissipation properties of TMDC materials which has relevance to potential electro-optical TMDC applications, in particular under strong optical or electronic excitation conditions.

Acknowledgements

The authors acknowledge financial support funded by the Deutsche Forschungsgemeinschaft (DFG, German Research Foundation) - Project number 277146847 - CRC 1238 and the support from the National Key Research and Development Program of China [Grant No. 2017YFA0304203]; National Natural Science Foundation of China (NSFC) [Grant Nos. 61605104, 61527824, 11434007]; PCSIRT [Grant No. IRT_17R70]; 111 project [Grant No. D18001] and 1331KSC; the Applied Basic Research Program of Shanxi Province (No. 2016021017).

References

[1] Novoselov K S, Geim A K, Morozov S V, Jiang D, Zhang Y, Dubonos S V, Grigorieva I V and Firsov A A 2004 Electric field effect in atomically thin carbon films *Science* 306 666-9

- [2] Ashton M, Paul J, Sinnott S B and Hennig R G 2017 Topology-Scaling Identification of Layered Solids and Stable Exfoliated 2D Materials *Phys Rev Lett* 118 106101
- [3] Coleman J N, Lotya M, O'Neill A, Bergin S D, King P J, Khan U, Young K, Gaucher A, De S, Smith R J, Shvets I V, Arora S K, Stanton G, Kim H Y, Lee K, Kim G T, Duesberg G S, Hallam T, Boland J J, Wang J J, Donegan J F, Grunlan J C, Moriarty G, Shmeliov A, Nicholls R J, Perkins J M, Grievson E M, Theuwissen K, McComb D W, Nellist P D and Nicolosi V 2011 Two-Dimensional Nanosheets Produced by Liquid Exfoliation of Layered Materials *Science* 331 568-71
- [4] Wang Q H, Kalantar-Zadeh K, Kis A, Coleman J N and Strano M S 2012 Electronics and optoelectronics of two-dimensional transition metal dichalcogenides *Nat Nanotechnol* 7 699-712
- [5] Geim A K and Grigorieva I V 2013 Van der Waals heterostructures *Nature* 499 419-25
- [6] Mak K F and Shan J 2016 Photonics and optoelectronics of 2D semiconductor transition metal dichalcogenides *Nat Photonics* 10 216-26
- [7] Xia F N, Wang H, Xiao D, Dubey M and Ramasubramaniam A 2014 Two-dimensional material nanophotonics *Nat Photonics* 8 899-907
- [8] Cao Q, Dai Y W, Xu J, Chen L, Zhu H, Sun Q Q and Zhang D W 2017 Realizing Stable p-Type Transporting in Two-Dimensional WS₂ Films *Acs Appl Mater Inter* 9 18215-21
- [9] Aji A S, Solis-Fernández P, Ji H G, Fukuda K and Ago H 2017 High Mobility WS₂ Transistors Realized by Multilayer Graphene Electrodes and Application to High Responsivity Flexible Photodetectors *Adv Funct Mater* 27 1703448
- [10] Komsa H P and Krasheninnikov A V 2012 Effects of confinement and environment on the electronic structure and exciton binding energy of MoS₂ from first principles *Phys Rev B* 86 241201(R)
- [11] Chernikov A, Berkelbach T C, Hill H M, Rigosi A, Li Y L, Aslan O B, Reichman D R, Hybertsen M S and Heinz T F 2014 Exciton Binding Energy and Nonhydrogenic Rydberg Series in Monolayer WS₂ *Phys Rev Lett* 113 076802
- [12] Zhu B R, Chen X and Cui X D 2015 Exciton Binding Energy of Monolayer WS₂ *Sci Rep* 5 9218

- [13] Park S, Mutz N, Schultz T, Blumstengel S, Han A, Aljarb A, Li L J, List-Kratochvil E J W, Amsalem P and Koch N 2018 Direct determination of monolayer MoS₂ and WSe₂ exciton binding energies on insulating and metallic substrates *2d Mater* 5 025003
- [14] Sim S, Park J, Song J G, In C, Lee Y S, Kim H and Choi H 2013 Exciton dynamics in atomically thin MoS₂: Interexcitonic interaction and broadening kinetics *Phys Rev B* 88 075434
- [15] Korn T, Heydrich S, Hirmer M, Schmutzler J and Schüller C 2011 Low-temperature photocarrier dynamics in monolayer MoS₂ *Appl Phys Lett* 99 102109
- [16] Sun D Z, Rao Y, Reider G A, Chen G G, You Y M, Brézin L, Harutyunyan A R and Heinz T F 2014 Observation of Rapid Exciton-Exciton Annihilation in Monolayer Molybdenum Disulfide *Nano Lett* 14 5625-9
- [17] Chernikov A, Ruppert C, Hill H M, Rigosi A F and Heinz T F 2015 Population inversion and giant bandgap renormalization in atomically thin WS₂ layers *Nat Photonics* 9 466-70
- [18] Yuan L and Huang L B 2015 Exciton dynamics and annihilation in WS₂ 2D semiconductors *Nanoscale* 7 7402-8
- [19] Pogna E A A, Marsili M, De Fazio D, Dal Conte S, Manzoni C, Sangalli D, Yoon D, Lombardo A, Ferrari A C, Marini A, Cerullo G and Prezzi D 2016 Photo-Induced Bandgap Renormalization Governs the Ultrafast Response of Single-Layer MoS₂ *Acs Nano* 10 1182-8
- [20] Schmidt R, Berghäuser G, Schneider R, Selig M, Tonndorf P, Malić E, Knorr A, de Vasconcellos S M and Bratschitsch R 2016 Ultrafast Coulomb-Induced Intervalley Coupling in Atomically Thin WS₂ *Nano Lett* 16 2945-50
- [21] Yu Y L, Yu Y F, Xu C, Barrette A, Gundogdu K and Cao L Y 2016 Fundamental limits of exciton-exciton annihilation for light emission in transition metal dichalcogenide monolayers *Phys Rev B* 93 201111(R)
- [22] Cunningham P D, McCreary K M and Jonker B T 2016 Auger Recombination in Chemical Vapor Deposition-Grown Monolayer WS₂ *J Phys Chem Lett* 7 5242-6
- [23] Nan F, Qiu Y H, Zhou L and Wang Q Q 2017 Ultrafast exciton dynamics in chemical heterogenous WSe₂ monolayer *J Phys D Appl Phys* 50 485109

- [24] Sie E J, Steinhoff A, Gies C, Luo C H, Ma Q, Rösner M, Schonhoff G, Jahnke F, Wehling T O, Lee Y H, Kong J, Jarillo-Herrero P and Gedik N 2017 Observation of Exciton Redshift-Blueshift Crossover in Monolayer WS₂ Nano Lett 17 4210-6
- [25] Jiang T, Chen R Z, Zheng X, Xu Z J and Tang Y H 2018 Photo-induced excitonic structure renormalization and broadband absorption in monolayer tungsten disulphide Opt Express 26 859-69
- [26] Kim J, Hong X P, Jin C H, Shi S F, Chang C Y S, Chiu M H, Li L J and Wang F 2014 Ultrafast generation of pseudo-magnetic field for valley excitons in WSe₂ monolayers Science 346 1205-8
- [27] Sie E J, McIver J, Lee Y H, Fu L, Kong J and Gedik N 2015 Valley-selective optical Stark effect in monolayer WS₂ Nat Mater 14 290-4
- [28] Sie E J, Lui C H, Lee Y H, Kong J and Gedik N 2016 Observation of Intervalley Biexcitonic Optical Stark Effect in Monolayer WS₂ Nano Lett 16 7421-6
- [29] Ruppert C, Chernikov A, Hill H M, Rigosi A F and Heinz T F 2017 The Role of Electronic and Phononic Excitation in the Optical Response of Monolayer WS₂ after Ultrafast Excitation Nano Lett 17 644-51
- [30] Kang K, Ozel T, Cahill D G and Shim M 2008 Optical Phonon Lifetimes in Single-Walled Carbon Nanotubes by Time-Resolved Raman Scattering Nano Lett 8 4642-7
- [31] Song D H, Wang F, Dukovic G, Zheng M, Semke E D, Brus L E and Heinz T F 2008 Direct measurement of the lifetime of optical phonons in single-walled carbon nanotubes Phys Rev Lett 100 225503
- [32] Saichu R P, Mahns I, Goos A, Binder S, May P, Singer S G, Schulz B, Risydi A, Unterhinninghofen J, Manske D, Guptasarma P, Williamsen M S and Rübhausen M 2009 Two-Component Dynamics of the Order Parameter of High Temperature Bi₂Sr₂CaCu₂O_{8+delta} Superconductors Revealed by Time-Resolved Raman Scattering Phys Rev Lett 102 177004
- [33] Yan H G, Song D H, Mak K F, Chatzakis I, Maultzsch J and Heinz T F 2009 Time-resolved Raman spectroscopy of optical phonons in graphite: Phonon anharmonic coupling and anomalous stiffening Phys Rev B 80 121403(R)

- [34] Nesbitt J M and Smith D C 2013 Measurements of the Population Lifetime of D Band and G' Band Phonons in Single-Walled Carbon Nanotubes *Nano Lett* 13 416-22
- [35] Zhu J, German R, Senkovskiy B V, Haberer D, Fischer F R, Grüneis A and van Loosdrecht P H M 2018 Exciton and phonon dynamics in highly aligned 7-atom wide armchair graphene nanoribbons as seen by time-resolved spontaneous Raman scattering *Nanoscale* 10 17975-82
- [36] Xu Z Q, Zhang Y P, Lin S H, Zheng C X, Zhong Y L, Xia X, Li Z P, Sophia P J, Fuhrer M S, Cheng Y B and Bao Q L 2015 Synthesis and Transfer of Large-Area Monolayer WS₂ Crystals: Moving Toward the Recyclable Use of Sapphire Substrates *Acs Nano* 9 6178-87
- [37] Fu Q, Wang W H, Yang L, Huang J, Zhang J Y and Xiang B 2015 Controllable synthesis of high quality monolayer WS₂ on a SiO₂/Si substrate by chemical vapor deposition *Rsc Adv* 5 15795-9
- [38] Versteeg R B, Zhu J, Padmanabhan P, Boguschewski C, German R, Goedecke M, Becker P and van Loosdrecht P H M 2018 A tunable time-resolved spontaneous Raman spectroscopy setup for probing ultrafast collective excitation and quasiparticle dynamics in quantum materials *Struct Dynamics* 5 044301
- [39] Gutiérrez H R, Perea-López N, Elías A L, Berkdemir A, Wang B, Lv R, Lopez-Urias F, Crespi V H, Terrones H and Terrones M 2013 Extraordinary Room-Temperature Photoluminescence in Triangular WS₂ Monolayers *Nano Lett* 13 3447-54
- [40] Zhao W J, Ghorannevis Z, Chu L Q, Toh M L, Kloc C, Tan P H and Eda G 2013 Evolution of Electronic Structure in Atomically Thin Sheets of WS₂ and WSe₂ *Acs Nano* 7 791-7
- [41] Mitioglu A A, Plochocka P, Jadczyk J N, Escoffier W, Rikken G L J A, Kulyuk L and Maude D K 2013 Optical manipulation of the exciton charge state in single-layer tungsten disulfide *Phys Rev B* 88 245403
- [42] Currie M, Hanbicki A T, Kioseoglou G and Jonker B T 2015 Optical control of charged exciton states in tungsten disulfide *Appl Phys Lett* 106 201907
- [43] Kobayashi Y, Sasaki S, Mori S, Hibino H, Liu Z, Watanabe K, Taniguchi T, Suenaga K, Maniwa Y and Miyata Y 2015 Growth and Optical Properties of High-Quality Monolayer WS₂ on Graphite *Acs Nano* 9 4056-63

- [44] Thripuranthaka M and Late D J 2014 Temperature Dependent Phonon Shifts in Single-Layer WS₂ *Acs Appl Mater Inter* 6 1158-63
- [45] Staiger M, Gillen R, Scheuschner N, Ochedowski O, Kampmann F, Schleberger M, Thomsen C and Maultzsch J 2015 Splitting of monolayer out-of-plane A₁'(1) Raman mode in few-layer WS₂ *Phys Rev B* 91 195419
- [46] Lee C, Jeong B G, Yun S J, Lee Y H, Lee S M and Jeong M S 2018 Unveiling Defect-Related Raman Mode of Monolayer WS₂ via Tip-Enhanced Resonance Raman Scattering *Acs Nano* 12 9982-90
- [47] Berkdemir A, Gutiérrez H R, Botello- Méndez A R, Perea- López N, Elías A L, Chia C I, Wang B, Crespi V H, López-Urías F, Charlier J C, Terrones H and Terrones M 2013 Identification of individual and few layers of WS₂ using Raman Spectroscopy *Sci Rep* 3 1755
- [48] Zhang X, Qiao X F, Shi W, Wu J B, Jiang D S and Tan P H 2015 Phonon and Raman scattering of two-dimensional transition metal dichalcogenides from monolayer, multilayer to bulk material *Chem Soc Rev* 44 2757-85
- [49] Kash J A, Tsang J C and Hvam J M 1985 Subpicosecond Time-Resolved Raman-Spectroscopy of Lo Phonons in Gaas *Phys Rev Lett* 54 2151-4
- [50] Tsen K T and Morkoç H 1988 Subpicosecond Time-Resolved Raman-Spectroscopy of Lo Phonons in Gaas-Alxga1-X as Multiple-Quantum-Well Structures *Phys Rev B* 38 5615-6
- [51] Chiashi S, Murakami Y, Miyauchi Y and Maruyama S 2008 Temperature dependence of Raman scattering from single-walled carbon nanotubes: Undefined radial breathing mode peaks at high temperatures *Jpn J Appl Phys* 47 2010-5
- [52] Goldstein T, Chen S Y, Tong J Y, Xiao D, Ramasubramaniam A and Yan J 2016 Raman scattering and anomalous Stokes-anti-Stokes ratio in MoTe₂ atomic layers *Sci Rep* 6 28024
- [53] Jellison G E, Lowndes D H and Wood R F 1983 Importance of Temperature-Dependent Optical-Properties for Raman Temperature-Measurements for Silicon *Phys Rev B* 28 3272-6
- [54] Maher R C, Hou J, Cohen L F, Le Ru E C, Hadfield J M, Harvey J E, Etchegoin P G, Liu F M, Green M, Brown R J C and Milton M J T 2005 Resonance contributions to anti-Stokes/Stokes ratios under surface enhanced Raman scattering conditions *J Chem Phys* 123 084702

- [55] Baranowski M, Surrente A, Maude D K, Ballottin M, Mitioglu A A, Christianen P C M, Kung Y C, Dumcenco D, Kis A and Plochocka P 2017 Dark excitons and the elusive valley polarization in transition metal dichalcogenides 2d Mater 4 025016
- [56] Molas M R, Faugeras C, Slobodeniuk A O, Nogajewski K, Bartos M, Basko D M and Potemski M 2017 Brightening of dark excitons in monolayers of semiconducting transition metal dichalcogenides 2d Mater 4 021003
- [57] Loh K P 2017 2D MATERIALS Brightening the dark excitons Nat Nanotechnol 12 837-8
- [58] Danovich M, Zólyomi V and Fal'ko V I 2017 Dark trions and biexcitons in WS₂ and WSe₂ made bright by e-e scattering Sci Rep 7 45998
- [59] Van der Donck M, Zarenia M and Peeters F M 2018 Strong valley Zeeman effect of dark excitons in monolayer transition metal dichalcogenides in a tilted magnetic field Phys Rev B 97 081109(R)
- [60] Carozo V, Wang Y X, Fujisawa K, Carvalho B R, McCreary A, Feng S M, Lin Z, Zhou C J, Perea-López N, Elías A L, Kabijs B, Crespi V H and Terrones M 2017 Optical identification of sulfur vacancies: Bound excitons at the edges of monolayer tungsten disulfide Sci Adv 3 1602813
- [61] Liu X, Hu J, Yue C, Della Fera N, Ling Y, Mao Z and Wei J 2014 High performance field-effect transistor based on multilayer tungsten disulfide Acs Nano 8 10396-402
- [62] Yuan L, Wang T, Zhu T, Zhou M and Huang L 2017 Exciton Dynamics, Transport, and Annihilation in Atomically Thin Two-Dimensional Semiconductors J Phys Chem Lett 8 3371-9
- [63] Nurfani E, Kurniawan R, Aono T, Takeda K, Shirai Y, Sutjahja I M, Rusydi A, Winata T, Takase K and Darma Y 2017 Defect-induced excitonic recombination in T_xZn_{1-x}O thin films grown by DC-unbalanced magnetron sputtering Jpn J Appl Phys 56 112101
- [64] Reid K R, McBride J R, La Croix A D, Freymeyer N J, Click S M, Macdonald J E and Rosenthal S J 2018 Role of Surface Morphology on Exciton Recombination in Single Quantum Dot-in-Rods Revealed by Optical and Atomic Structure Correlation Acs Nano 12 11434-45